Timelike Compton Scattering

R. Paremuzyan,[1] N. Dashyan,[1] T. Horn,[2] Y. Ilieva,[3] F.J. Klein,[4] P. Nadel-Turonski,[4] C. Salgado,[5] and S. Stepanyan[†2]

[1] *Yerevan Physics Institute, 375036 Yerevan, Armenia*

[2] *Thomas Jefferson National Accelerator Facility, Newport News, Virginia 23606*

[3] *University of South Carolina, Columbia, South Carolina 29208*

[4] *Catholic University of America, Washington, D.C. 20064*

[5] *Norfolk State University, Norfolk, Virginia 23504*

(Dated: August 11, 2009)

We propose to analyze CLAS e1-6 and e1f data sets in order to study Compton scattering in the time-like region. This is interesting in particular for extracting the real part of the Compton amplitude. At high virtualities, photoproduction of lepton pairs (l^+l^-) is an inverse process to Deeply Virtual Compton Scattering (DVCS) and gives access to Generalized Parton Distributions (GPDs). In Time-like Compton Scattering (TCS), the real part of the Compton amplitude can be accessed via measuring an asymmetry arising from exchange of l^+ and l^- momenta. The real part is proportional to the integral of GPDs over the internal quark loop momentum, x, and will provide important information for modeling the GPDs, in particular the contribution of the D-term.

The process that will be analyzed is quasi-real photoproduction of (e^+e^-) pairs at high virtualities ($m^2_{e^+e^-} = Q'^2 > 1.1$ GeV^2) in the reaction $e(p, e^+e^-p')e'$, where e and e' are incoming (beam) and scattered electrons, p and p' are the target and recoil nucleons, and e^+ and e^- are the final state lepton pairs. The experiment will detect p', e^+, and e^-. The kinematics of the scattered electron will be deduced from missing momentum analysis. In order to have photoproduction of lepton pairs, events with electrons scattered at very small angles will be selected. The real part of the Compton amplitude will be extracted from the azimuthal angular asymmetry between the reaction plane and the lepton plane. If statistics permits, the imaginary part of the Compton amplitude will be studied using the

[†] Contact person

beam helicity dependent asymmetry (with circularly polarized photons).

Contents

I. INTRODUCTION

Much of the internal structure of the nucleon has been revealed during the past three decades through *inclusive* scattering of high-energy leptons on nucleons in the Bjorken or Deeply Inelastic Scattering (DIS)- regime. Simple theoretical interpretations of the experimental results and quantitative conclusions can be reached within the framework of the parton model and QCD when one sums over all possible hadronic final states. For instance, *unpolarized* DIS led to the discovery of the quark and gluon substructure of the nucleon, with the quarks carrying about half of the nucleon's momentum. Furthermore, *polarized* DIS revealed that only about 25% of the spin of the nucleon originates from the intrinsic spin of the quarks. However, very little is known about quark-quark correlations, the transverse momentum distribution of the quarks, and contributions of correlated quark-antiquark pairs (mesons) to the nucleon wave function.

The recently developed formalism of Generalized Parton Distributions (GPDs)[1, 2] showed that such information can be obtained in hard *exclusive* leptoproduction experiments. The GPDs contain information on the interference between different quark configurations, on the quark transverse momentum distribution, as well as on their angular momentum distribution [3]. GPDs provide a unifying picture for an entire set of fundamental quantities characterizing the hadronic structure, such as: the vector and axial vector nucleon form factors, the polarized and unpolarized parton distributions, and the spin components of the nucleon due to orbital excitations.

Deeply Virtual Compton Scattering (DVCS) is one of the key reactions for determining the GPDs experimentally, and it is the simplest process that can be described in terms of GPDs. The spin asymmetries in DVCS give access to the imaginary part of the scattering amplitude, where GPDs enter at specific kinematical point. A broader surface can be mapped out in the double DVCS process, when both the incoming and the outgoing photons have large virtualities.

The real part of the amplitude, which contains integrals of GPDs along quark internal loop momentum, is not directly accessible through the spin observables. It can be accessed either in cross section measurements or in beam charge asymmetry measurements (requiring lepton beams of both charges). Extracting the real part of the Compton amplitude is important for constraining models of GPDs.

We propose here to study the inverse process to DVCS, the Timelike Compton Scattering (TCS), when the incoming photon is real and the outgoing photon has a large virtuality (production of heavy lepton pairs (l^+l^-)). As in the case of DVCS, there is an interference between TCS and the Bethe-Heitler (BH) process. This interference will project out the real part of the Compton amplitude in the azimuthal angular asymmetry of lepton pair production with unpolarized photons. We will analyze the reaction $ep \rightarrow e^+e^-p'(e')$ using the e1-6 and e1f data sets. The scattered electron (e') will not be detected. Its kinematics will be deduced from missing momentum analysis. TCS events will be selected by requiring the electron scattering angle to be very small ($\theta_e \sim 0$, quasi-real photoproduction). The invariant mass distribution and the angular asymmetries of lepton pairs will be studied in a wide range of kinematics. Final results from the angular asymmetries will be compared to model calculations.

II. PHYSICS MOTIVATION

Hard scattering processes play an important role in the understanding of the quark and gluon structure of hadrons. The important feature of hard reactions is the possibility of separating the perturbative (short distance) and the non-perturbative (long distance) parts of the strong interaction. This so-called factorization property has been successfully used in inclusive measurements (*e.g.*, in Deep Inelastic Scattering (DIS) of leptons) to study the internal structure of the nucleon. Until recently, very few exclusive processes could be treated in the framework of pQCD and be compared to experimental data (typical examples are the $\pi^0\gamma\gamma^*$ transition form factor [4] and the elastic form factors of the pion [5] and the nucleon [6]). The recently developed formalism of a QCD description of Deeply Virtual Compton Scattering (DVCS) [1, 2] and Deeply Exclusive Meson Production [7], provides a framework in which the amplitudes of these processes can be factorized into a hard-scattering part (exactly calculable in pQCD), and a non-perturbative nucleon structure part that can be parameterized at the amplitude level by means of Generalized Parton Distributions (GPDs), see Fig. 1. The GPDs contain information on quark/antiquark correlations, particularly the correlation of their transverse spatial and longitudinal momentum distributions, and on the quark angular momentum [3]. They provide a unifying picture for an entire set of fundamental

quantities containing information on the hadronic structure, such as nucleon form factors (which are related to the matrix elements of vector and axial vector currents), polarized and unpolarized parton distributions, and contributions to the spin of the nucleon due to orbital excitations of quarks and gluons.

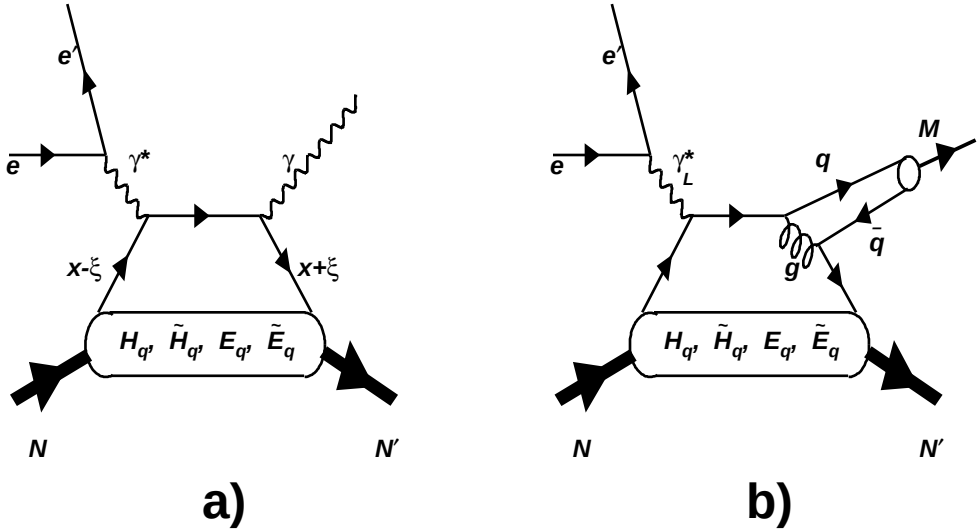

FIG. 1: "Handbag" diagrams for: (a) DVCS, (b) meson production.

A. Phenomenology of the GPDs

There are four chiral-even GPDs, denoted by H^q, $\tilde{H}^q$, E^q, and $\tilde{E}^q$, which depend on the kinematical variables x, ξ, and t. They correspond to the amplitude for removing a quark with momentum fraction $x-\xi$ and restoring it with momentum fraction $x+\xi$ (Fig. 1.a). The light-cone momentum fraction x is defined by $\kappa^+ = x\bar{P}^+$, where κ is the quark loop momentum and $\bar{P}$ is the average nucleon momentum ($\bar{P} = (p'+p)/2$, where p and p' are the initial and final state nucleon four-momenta, respectively). ξ is the Generalized Bjorken variable: $\xi = Q^2/(4q\cdot\bar{P}) \to x_B/(2-x_B)$ as $t/Q^2 \to 0$, where $q = k-k'$, $Q^2 = -q^2$, and k and k' are the initial and final electron momenta.

The Mandelstam variable $t = (p'-p)^2$ is the Lorentz-invariant four-momentum transfer squared

to the target. In the forward limit where $t \to 0$, the GPDs H and $\tilde{H}$ reduce to the quark density distributions $q(x)$ and quark helicity distributions $\Delta q(x)$ obtained from DIS:

$$H^q(x,0,0) = \begin{cases} q(x), & x > 0 \\ -\bar{q}(-x), & x < 0 \end{cases} \tag{1}$$

$$\tilde{H}^q(x,0,0) = \begin{cases} \Delta q(x), & x > 0 \\ \Delta\bar{q}(-x), & x < 0\,. \end{cases} \tag{2}$$

E and $\tilde{E}$ are accessible through hard exclusive electroproduction reactions only and are new leading-twist functions. In DIS, that corresponds to the limit $\xi \to 0$, the region $-\xi < x < \xi$ is absent. In this region GPDs behave like meson distribution amplitudes and contain completely new information about nucleon structure. At finite momentum transfer, the first moments of GPDs are related to the elastic form factors of the nucleon through model independent sum rules. By integrating over x one can obtain for a particular quark flavor (for any ξ):

$$\int_{-1}^{+1} dx H^q(x,\xi,t) = F_1^q(t) \tag{3}$$

$$\int_{-1}^{+1} dx E^q(x,\xi,t) = F_2^q(t) \tag{4}$$

$$\int_{-1}^{+1} dx \tilde{H}^q(x,\xi,t) = g_A^q(t) \tag{5}$$

$$\int_{-1}^{+1} dx \tilde{E}^q(x,\xi,t) = h_A^q(t), \tag{6}$$

where $F_1^q(t)$ and $F_2^q(t)$ represent the elastic Dirac and Pauli form factors for the quark flavor q in the nucleon, g_A^q is the axial-vector form factor of the nucleon, and h_A^q is the pseudo-scalar form factor.

B. Revealing GPDs

From a phenomenological point of view, the extraction of the GPDs from experimental data is not a simple task. It requires an extensive experimental program and detailed analysis with controlled theoretical corrections. Although the field is rapidly expanding, we expect that, as a first step, phenomenological parameterizations of GPDs will be used to fit the experimental data. Existing parameterizations include general constraints that are derived from DIS and form factor measurements. One of the commonly used parameterizations utilizes a factorized ansatz for the t-distribution, and defines the t-independent part of the GPD as a sum of two terms (*e.g.*, for H^q):

$$H^q(x,\xi) \;=\; H^q_{DD}(x,\xi) \;+\; \theta(\xi-|x|)\,\frac{1}{N_f}\,D(\frac{x}{\xi})\,, \tag{7}$$

where H^q_{DD} is the part of the GPD that is obtained as a one-dimensional section of a two-variable double distribution (DD) [8]. The second term in Eq. (7), the so-called D-term [9], is introduced to ensure the non-trivial properties of GPDs: the polynomiality of their Mellin moments [1]. In Figure 2, two models of the GPD H at $t = 0$ are presented. The two surfaces correspond to models without (left-hand surface) and with (right-hand surface) the D term in the parameterization. There are several parameterizations of the t-dependence of the GPDs. One of early parametrization uses factorized ansatz, where t-dependence is parameterized in terms of the Dirac form factor $F_1^q(t)$ for a quark flavor q, determined through empirical parameterizations of the proton and the neutron Dirac form factors:

$$H^q(x,\xi,t) \;=\; H^q(x,\xi)F_1^q(t), \tag{8}$$

Studies of nucleon form factors from generalized parton distributions, presented in [10], showed that the x- and t-dependences of GPDs are coupled and introduced Regicide parametrization of the t-dependence of GPDs in a form $x^{-\alpha' t}$. Here α' is the only parameter and corresponds to the slope of the Regge trajectory in the vector EM current channel.

Using such models, experimentally accessible quantities can be calculated and compared with the measurements. Quark flavor separation of GPDs requires systematic studies using both proton and neutron (deuterium) targets, and measurements of the production of different meson species. Reactions with vector or scalar mesons in the final state are sensitive to unpolarized (H and E) or polarized ($\tilde{H}$ and $\tilde{E}$) GPDs, respectively.

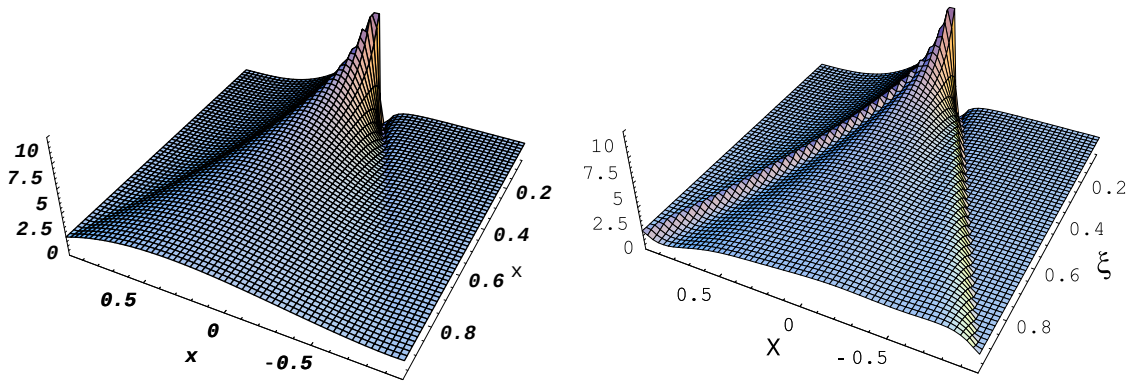

FIG. 2: Model calculations of the GPD H as a function of ξ and x at $t = 0$. The left-hand surface is a model without the D-term in the t-independent part of the parameterization. The right-hand surface includes the D-term in the parameterization [9]. DIS measures a line at $\xi = 0$. For $x > 0$, the distribution corresponds to quarks, and for $x < 0$ it corresponds to antiquarks.

C. Accessing GPDs Experimentally

Deeply Virtual Compton Scattering, $ep \to ep\gamma$, is the simplest reaction to access GPDs experimentally and much of the progress to date in studying the GPDs experimentally comes from the DVCS measurements. The azimuthal dependence of the beam spin asymmetry (BSA) has been measured by the CLAS [13] and HERMES [14] collaborations with electron (4.25 GeV) and positron (27.6 GeV) beams, respectively. The longitudinal target-spin asymmetry has been reported by CLAS [15]. The Q^2 dependence of the helicity-dependent and helicity-independent cross sections were measured on the proton [16] and on the neutron [17] (deuterium target) by the Hall A Collaboration at Jefferson Lab. The HERMES collaboration reported also the first measurement of the lepton beam charge asymmetry (BCA) [18]. Recently, CLAS collaboration published measurements of DVCS beam spin asymmetry over a wide kinematical range using high statistics data obtained with 5.77 GeV longitudinally polarized electron beam [19]. There are also data on unpolarized cross sections from HERA [20] and results on a transversely polarized target from HERMES [21].

GPDs enter in the Compton formfactors (CFFs) as integrals over x, and therefore only ξ and t are accessible (omitting summation over the quark species):

$$\{\mathcal{H}, \mathcal{E}, ...\}(\xi, t) = \int_{-1}^{1} dx\, C^{(\pm)}(\xi, x)\, \{H, E, ...\}(x, \eta, t)_{|\eta=-\xi}\,, \tag{9}$$

where "..." denotes other similar twist-two and twist-three GPDs. Coefficient functions $C^{(\pm)}$ for the even and odd parity sectors are given by (at 0th order in α_s):

$$\xi\, C^{(\mp)}_{(0)i}\,(\xi, x) = \frac{Q_i^2}{1 - x/\xi - i0} \mp \frac{Q_i^2}{1 + x/\xi - i0}\,. \tag{10}$$

Integration in Eq. (9) defines the real part of the Compton amplitude, for example for GPD H, as:

$$Re\ \mathcal{H}(\xi, t) = PV \int_{-1}^{1} dx\, C^{-}(\xi, x) H(x, \xi, t)\,, \tag{11}$$

and the imaginary part as:

$$Im\ \mathcal{H}(\xi, t) = i\pi H(\xi, \xi, t)\,. \tag{12}$$

Spin asymmetries in DVCS will project out the imaginary part of the Compton amplitude and hence access to the GPDs at the specific kinematic point, $x = \xi$. The real part of the Compton amplitude can be accessed directly in the lepton beam charge asymmetry measurements. Measurements of the DVCS cross section (at the kinematics where DVCS contribution is dominant) will allow determination of the square of the real part of the amplitude ($|Re|^2$) [11, 12]. Combinations of single (target or beam) and double spin asymmetries, cross sections, and lepton beam charge asymmetries will be needed for studying the GPDs using DVCS measurements. Quark flavor separation of GPDs requires systematic studies using both proton and neutron targets.

A program for a global fit to the DVCS data to extract the GPDs from a complex set of experimental observables is presented in [22]. Authors used nine independent observables to fit eight (seven, assuming $Im\tilde{E} = 0$) quantities (four imaginary and four real parts of Compton FFs). The conclusion of fits with simulated and real data are that with enough observable it is possible to constrain seven GPDs. Also, it might be possible to reduce the number of independent parameters using model motivated ansatzes or dispersion relations.

The experimental field is rapidly growing. More data on DVCS with polarized beams and targets are expected from 6 GeV experiments at JLAB/CLAS and orders of magnitude more after the 12 GeV upgrade. Nonetheless, DVCS measurements alone will not be enough to fully constrain the GPDs experimentally. There are two issues to be addressed: (1) determination of GPDs at $x \neq \xi$ points (spin asymmetries will define GPDs at $x = \xi$ point, a ridge on the x vs. ξ surface); (2) reliable extraction of the real part of the CFFs.

The first point, mapping out the surface of GPDs and not only $x = \xi$ line, can be achieved by measuring Double DVCS process. DDVCS is a process when the final state photon has time like virtuality and decays to a lepton pair [23, 24]. Virtuality of the outgoing photon allows to vary x and ξ independently. However, one should note that the cross section of the DDVCS process is reduced by few orders of magnitude compare to DVCS at given incoming photon virtuality and identifying the reaction in the decay mode of the outgoing virtual photon to e^+e^- has an ambiguity due to two electrons in the final state.

For the second point, as was shown in [22], extraction the real part of the Compton amplitudes can be reliably done from BCA measurement or by analysis of combinations of BCA and/or several longitudinal and transverse beam and/or target asymmetry measurements and cross section measurement. The BCA requires the use of lepton beams with both charges. The combined analysis of different spin asymmetries measured in different experiments, can potentially have large systematic uncertainties and requires a huge amount of statistics.

One of the important aspects of measuring the real part of the Compton amplitude is the sensitivity to the D-term introduced in the modeling of GPDs [8, 9]. The only BCA measurement so far has been published by the HERMES collaboration [18]. Their analysis gives a positive asymmetry of the order of 0.1. Although in this measurement the reaction channel is not exclusive and the statistical errors are large, the comparison of the obtained asymmetry to the model calculations reviles the importance of the D-term in the parameterization of GPDs.

The information on the real part of the scattering amplitude can also be obtained from photoproduction of heavy lepton pairs (see Fig. 3). This process, called Timelike Compton Scattering [25, 26], is an inverse process to DVCS and shares many of its features. In the case of TCS, the BH process also contributes at the amplitude level, and therefore linear combinations of GPDs can be accessed through BH-TCS interference.

III. TIME-LIKE COMPTON SCATTERING

A detailed evaluation of the TCS process and numerical estimates for various observables in our energy range is provided in Ref. [25]. As in the case of DVCS, the Compton subprocess -

$$\gamma(q) + p(p) \to \ell^-(k) + \ell^+(k') + p(p') \tag{13}$$

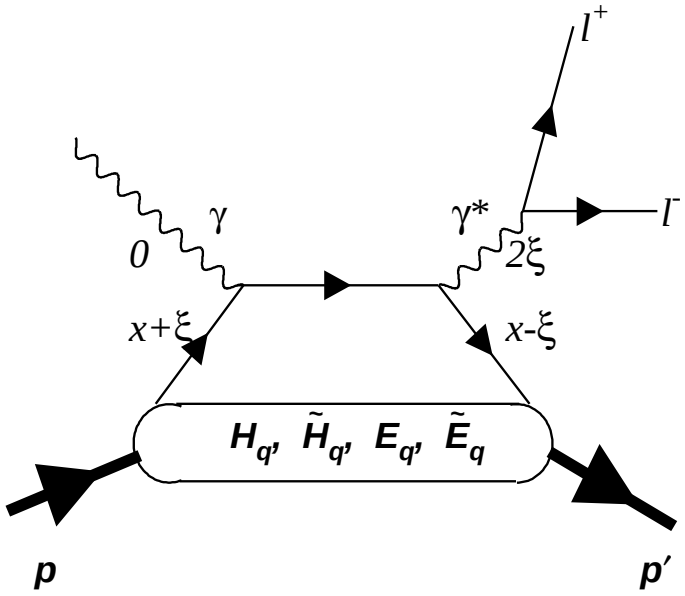

FIG. 3: "Handbag" diagram for heavy lepton pair photoproduction, called Timelike Compton Scattering.

interferes with the Bethe-Heitler process as shown in Fig. 4. In Eq.(13), q and p are the four-momenta of the incoming photon and the target nucleon, while k and k' are the four-momenta of the negatively and the positively charged leptons, respectively. The four-momentum of the scattered nucleon is denoted by p'.

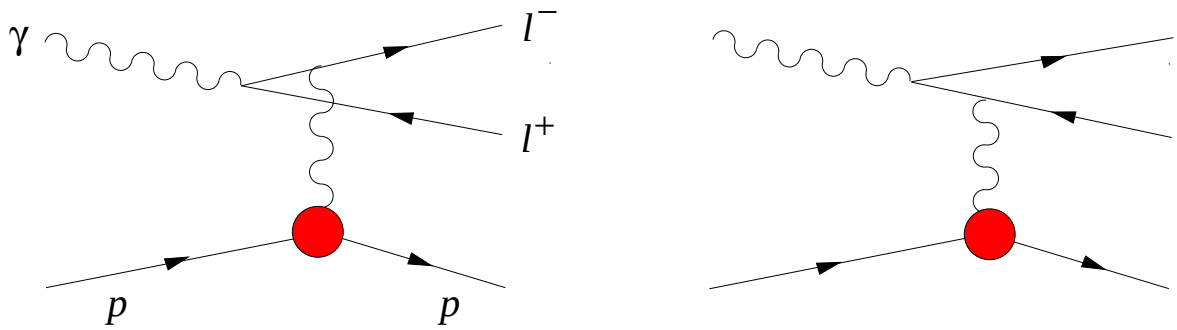

FIG. 4: Feynman diagrams for the Bethe-Heitler amplitude.

The suitable kinematic variables to describe the production of lepton pairs are θ, the polar angle

of ℓ^- in the c.m. of the lepton pair (with the z-axis pointing in the opposite direction to that of the scattered nucleon) and ϕ, the azimuthal angle between the lepton and the scattering planes as shown in Fig. 5. The azimuthal angle plays the same role as its analog in DVCS, and is the key for obtaining information on Compton scattering from its interference with the Bethe-Heitler process.

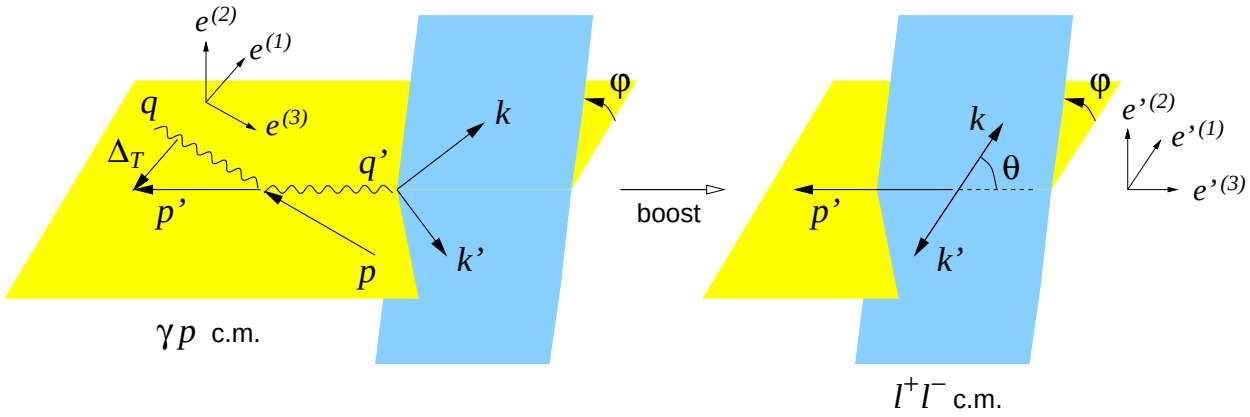

FIG. 5: Sketch of the kinematical variables and coordinate axes in the γp and $\ell^+\ell^-$ c.m. frames.

To filter out the interference term one can use the fact that the e^+e^- pair is produced in a C odd state by Compton scattering, and in a C even state by the Bethe-Heitler process. Any observable that changes sign under the exchange of e^- and e^+ momenta hence projects out the BH-TCS interference. The azimuthal asymmetry is the analog of the beam charge asymmetry in DVCS, and it is readily available from the angular distribution of the leptons instead of requiring beams of opposite charge. The interference part of the cross section for $\gamma p \to e^+e^-p$ with unpolarized protons and photons is given by ([25]):

$$\frac{d\sigma_{INT}}{dQ'^2\, dt\, d(\cos\theta)\, d\varphi} = -\frac{\alpha_{em}^3}{4\pi s^2}\frac{1}{-t}\frac{M}{Q'}\frac{1}{\tau\sqrt{1-\tau}}\frac{L_0}{L}\left[\cos\varphi\,\frac{1+\cos^2\theta}{\sin\theta}\,Re\tilde{M}^{--} - \cos 2\varphi\,\sqrt{2}\cos\theta\,Re\tilde{M}^{0-} + \cos 3\varphi\,\sin\theta\,Re\tilde{M}^{+-} + O\Big(\frac{1}{Q'}\Big)\right], \tag{14}$$

with L and L_0 defined as:

$$L = \Big[(q-k)^2 - m_e^2\Big]\Big[(q-k')^2 - m_e^2\Big] = \frac{(Q'^2-t)^2 - b^2}{4}, \tag{15}$$

$$L_0 = \frac{Q'^4\sin^2\theta}{4}, \tag{16}$$

where $b = 2(k - k') \cdot (p - p')$.

Quark hand-bag diagrams (Fig. 3) only generate helicity conserving transitions between transverse photons, and hence in Eq.(14) the leading term is $Re\tilde{M}^{--}$. In the scaling regime $Re\tilde{M}^{--}$ can be analyzed in terms of GPDs:

$$\tilde{M}^{--} = \frac{2\sqrt{t_0 - t}}{M} \frac{1-\eta}{1+\eta} \left[F_1 \mathcal{H}_1 - \eta(F_1 + F_2)\, \tilde{\mathcal{H}}_1 - \frac{t}{4M^2} F_2\, \mathcal{E}_1 \right], \tag{17}$$

where $-t_0 = 4\eta^2 M^2/(1-\eta^2)$ is the minimal value of $-t$ at given η, up to corrections in $1/Q'^2$, and $\eta = (p - p')^+/(p + p')^+$ is the plus-momentum fraction.

$Re\tilde{M}^{--}$ can be projected out by weighting differential cross section with $(L/L_0)\cos\phi$. Experimentally, it is simpler to measure the ratio of the Fourier coefficients

$$R(\sqrt{s},\ Q'^2,\ t) = \frac{2\displaystyle\int_0^{2\pi} d\varphi\, \cos\varphi \frac{dS}{dQ'^2\, dt\, d\varphi}}{\displaystyle\int_0^{2\pi} d\varphi \frac{dS}{dQ'^2\, dt\, d\varphi}}\,, \tag{18}$$

Here the weighted cross section S is defined as:

$$\frac{dS}{dQ'^2\, dt\, d\varphi} = \int_{\pi/4}^{3\pi/4} d\theta\, \frac{L(\theta,\varphi)}{L_0(\theta)} \frac{d\sigma}{dQ'^2\, dt\, d\theta\, d\varphi}\,. \tag{19}$$

The integration range is limited to $\{\pi/4,\ 3\pi/4\}$ to cut out regions where the TCS contribution is extremely small compared to BH contribution.

Numerical estimates for the ratio R defined in Eq.(18) are given in [25] for kinematics at $\sqrt{s} = 5$ GeV and $Q'^2 = 5$ GeV^2 as a function of $-t$. For different contributions of the D-term, R changes in the range from a few to 10%.

In this analysis, the ratio R defined in Eq.(18) will be studied as a function of $-t$ in the kinematical region $\sqrt{s} \simeq 3$ GeV and $Q'^2 = 1.7$ GeV^2.

IV. DATA SETS

Two data sets, from the e1-6 and e1f runs, are used in this analysis. Both are high-energy electroproduction experiments with standard CLAS detector settings using a liquid hydrogen target.

The e1-6 experiment ran from October 2001 until January 2002, using a 5.75 GeV longitudinally polarized electron beam. The beam polarization was measured using the Hall B Moller setup to

be $\sim$ 72%. For triggering the DAQ system, the CLAS electron trigger was used, requiring a coincidence of the forward electromagnetic calorimeter (EC) and Cherenkov counters (CC) in each sector($EC_i \otimes CC_i$, where $i = 1,..,6$ indicates CLAS sector number). The CLAS torus magnet current was set to 3375 A. The mini-torus current was set to 6000 A. The center of the 5 cm long LH_2 target was at the nominal CLAS center. During the run a total of 21 mC charge was accumulated on the Faraday cup.

The e1f experiment took place in April-July of 2003. The beam energy was 5.48 GeV. The electrons were longitudinally polarized. The CLAS torus magnet current was set to 2250 A, and the mini-torus current was set to 6000 A. The center of a 5 cm long LH_2 target was 25 cm upstream of the nominal CLAS center. The standard CLAS electron trigger was used to trigger DAQ system. The total accumulated luminosity during this run was 21 fb$-$1.

V. QUASI-REAL PHOTOPRODUCTION OF e^+e^- PAIRS IN ELECTROPRODUCTION EXPERIMENT

In the production of e^+e^- pairs with an electron beam, there are two electrons in the final state. One is the electron scattered off the target, and the second electron is a decay product of the produced virtual photon. Photoproduction of e^+e^- pairs is studied in the reaction:

$$e \ + \ p \rightarrow e^+ \ + \ e^- \ + \ p' \ + \ (e'^-)\,, \tag{20}$$

where e^+e^- are product of the decay of the outgoing virtual photon, p' is the recoil proton, and the e'^- is the scattered electron. Originally, this reaction was studied in [27] from e1-6 data set in order to extract information on DDVCS. In [27], the detected electron was assumed to be the scattered electron. However, as was realized in the course of that analysis, in most of the events detected electron is from the decay of the outgoing virtual photon.

In this analysis, in order to select quasi-real photoproduction of lepton pairs, events with electrons scattered at very small angles ($\sim 0^\circ$) must be selected. It is assumed that the detected electron is from the decay of the outgoing virtual photon and the scattered electron kinematics is deduced from the missing momentum analysis of the (e^+e^-p') system.

A. PID

For electron and positron ID, cuts on the energy deposited in the EC (inner and total) and on the number of photoelectrons in the CC were applied. Distributions of the energy measured in EC normalized to the momentum of lepton candidates measured by tracking are shown in Fig. 6 for e^+ and e^- in the e1-6 data sample. Cuts are indicated by the vertical lines. Each graph is plotted after applying the cuts on the other two. The corresponding distributions for the e1f sample are shown in Fig. 7.

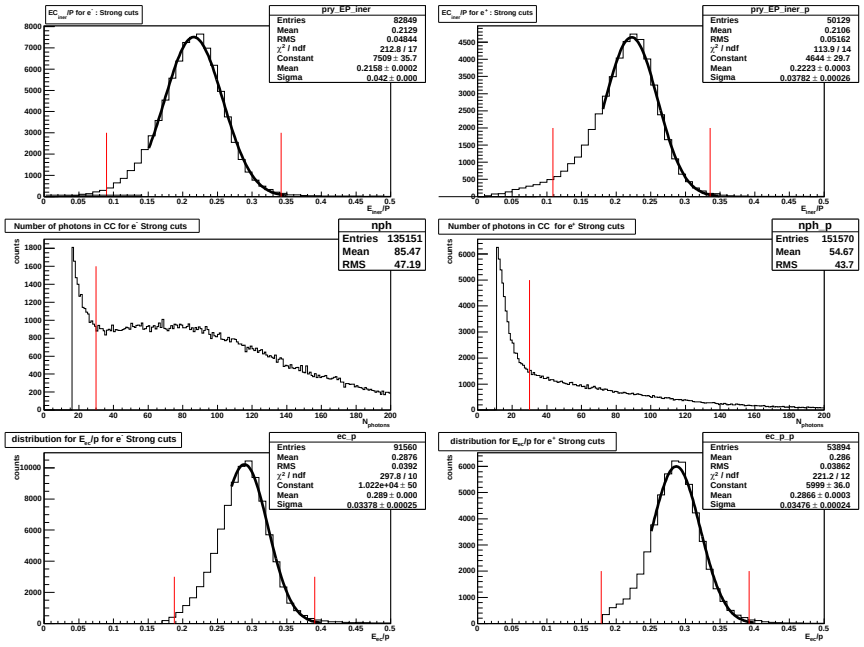

FIG. 6: Cuts for e^- (left) and e^+ (right) identification for the e1-6 data set. The top graphs correspond to EC inner energy, bottom graphs are for EC total energy. The distributions of the number of photoelectrons in the CC are shown in the middle graphs. Each distribution is plotted after cuts on other two (shown with red lines).

For proton identification, tracks with SEB PID=2212 are selected. Figure 8 shows the distribution of the energy deposited in the TOF counters by proton candidates as a function of particle momentum (the left graph is for the e1-6 and the right graph is for the e1f data sample). Protons produced in TCS have $P < 1$ GeV/c. As one can see, the selected tracks with momentum below 1 GeV/c are all protons.

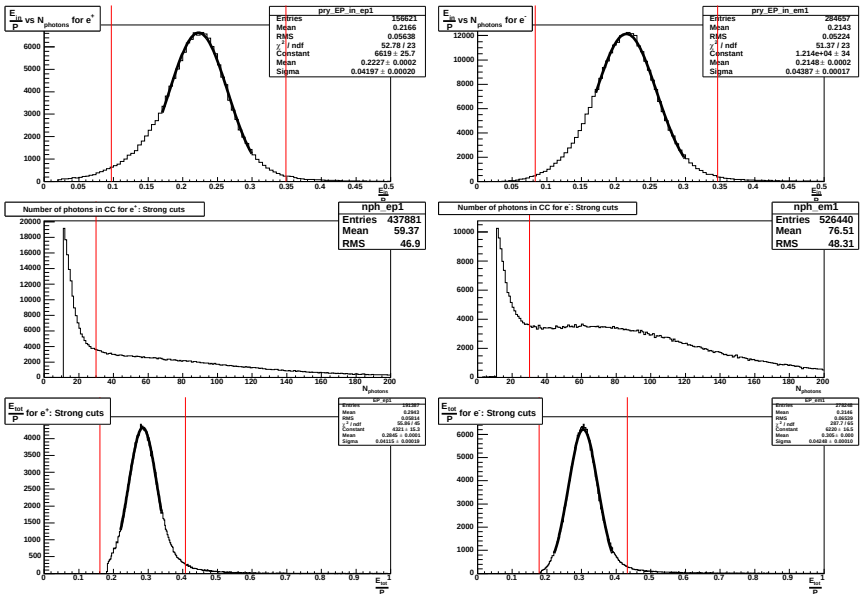

FIG. 7: Cuts for e^+ (left) and e^- (right) identification for the e1f data set. The distributions are the same as in the case of e1-6.

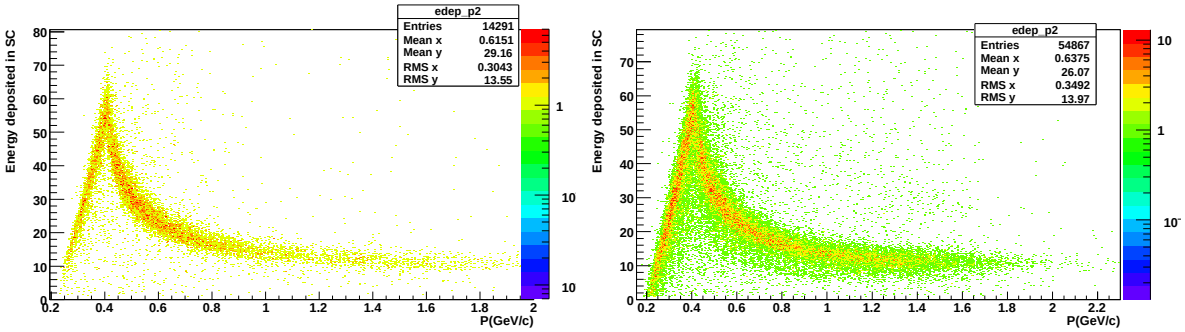

FIG. 8: Distribution of energy deposited by protons in the TOF for selected e^+e^-p events.

B. Final state identification

After applying PID cuts, missing momentum analysis for the final state e^+e^-p is performed. Figure 9 shows the distribution of the X and the Y components of the missing momentum (P_m^X and P_m^Y) normalized to the total missing momentum (P_m). *From hereon the left graph in the figures corresponds to e1-6 analysis and the right graph corresponds to e1f.* The strong enhancement at zero corresponds to events when the missing particle escaped in the direction of the beam. The distribution of the transverse component of the missing momentum, defined as $P_\perp/P_m = \sqrt{(P_m^X/P_m)^2 + (P_m^Y/P_m)^2}$, vs missing mass squared (MM^2) is shown in Fig. 10. The enhancement around $P_\perp = 0$ and $MM^2 = 0$ corresponds to events when the incoming electron scattered at very small angles. These are events corresponding to quasi-real photoproduction of e^+e^- pairs in the reaction $ep \rightarrow e^+e^-p'(e')$. The distribution of MM^2 vs photon energy ($E_\gamma = E_0 - E_m$, where E_0 is the electron beam energy and E_m is the missing energy) is shown in Fig. 11. In order to select TCS events, cuts on $P_\perp/P_m < 0.05$ and $|MM^2| < 0.05\text{GeV}^2$ for e1f, and $|MM^2| < 0.1$ GeV^2 for e1-6 are applied.

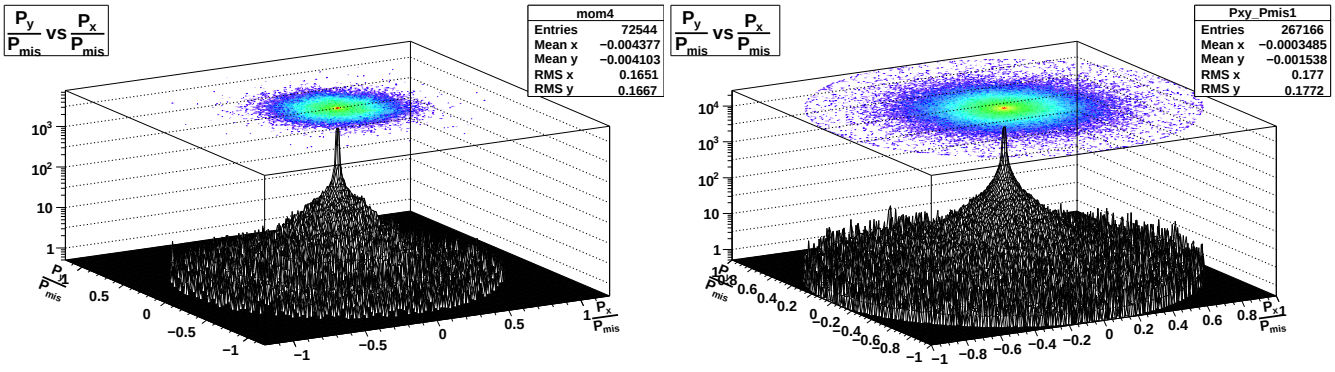

FIG. 9: Distributions of Y fraction of the missing three momentum vs. X fraction of missing momentum for selected e^+e^-p events for the e1-6 (left) and e1 (right), data sets.

In Fig. 12, $P_\perp/P_m$ distributions are shown with a fit to the peak at zero using a Gaussian plus polynomial function. The standard deviation of the Gaussian functions for both distributions, e1-6 and e1f, is $\simeq 0.004$. This means that 95% of selected events have the primary electron scattered at $< 0.5°$.

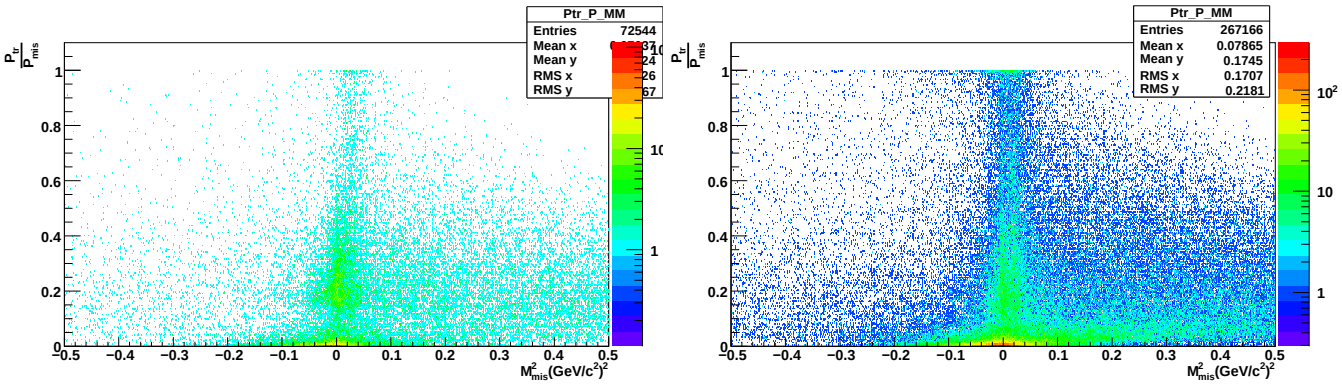

FIG. 10: Distribution of perpendicular momentum fraction vs. missing mass square for selected e^+e^-p events for e1-6, (left) and e1f (right) data sets.

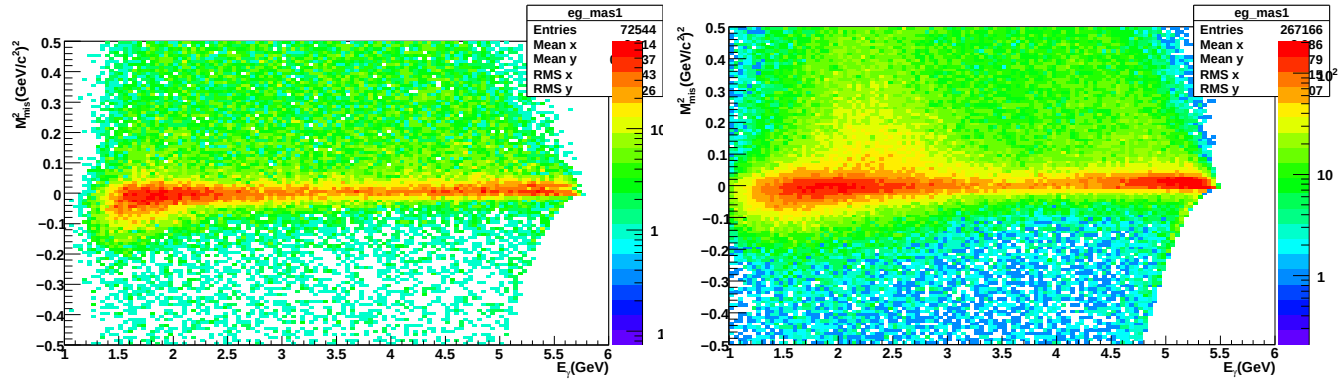

FIG. 11: Distribution of the missing mass square as a function of quasi-real photon energy for e1-6, (left) and e1f (right).

C. Selection of TCS event

After applying the cuts above, events in the reaction $\gamma p \rightarrow e^+e^-p$ are cleanly selected. The invariant mass distributions of the e^+e^-pairs in Fig. 13 show clear peaks corresponding to $\omega(782)$ and $\phi(1020)$ mesons decaying to e^+e^-(decay branching ratios are 7.16×10^{-5} and 2.97×10^{-4} [28], respectively). The broad distribution under the $\omega(782)$ peak is from $\rho(770) \rightarrow e^+e^-$ ($Br = 4.71 \times 10^{-5}$). These distributions are very similar to what was observed in the photoproduction of e^+e^-pairs in [29]. While production of these mesons in the time-like region is interesting by itself, and will be subject of further studies, in this analysis only the mass region above the ϕ meson will

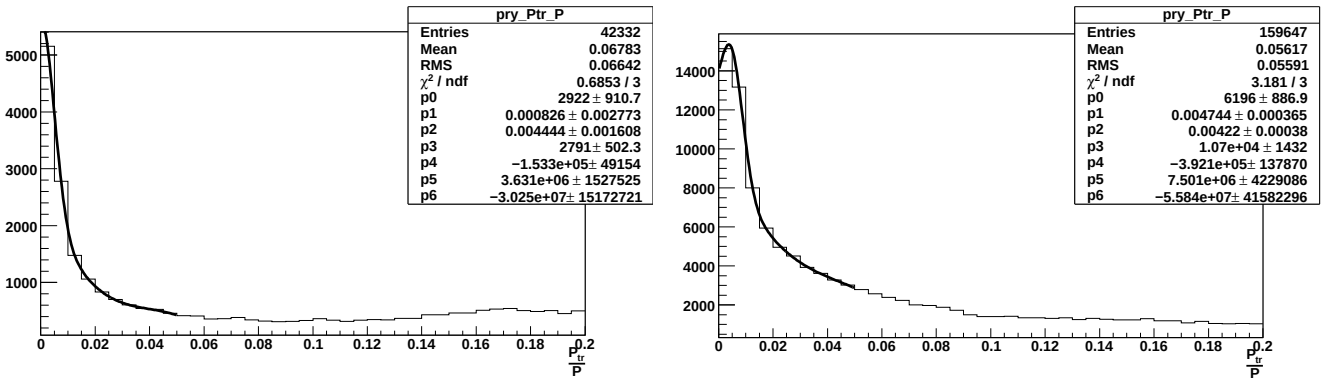

FIG. 12: Distribution of $P_\perp/P_m$ and fit to the peak at 0 with a Gaussian function. The tail is fitted with a polynomial. On the left is the distribution for e1-6, on the right, the corresponding one for e1f.

be considered. The e^+e^- invariant mass distribution vs the energy of the quasi-real photon (E_γ) is shown in Fig. 14. The region $M(e^+e^-) > 1.1$ GeV corresponds to $E_\gamma > 2$ GeV and defines kinematics of TCS analysis at $\sqrt{s} > 1.7$ GeV and $Q'^2 > 1,2$ (GeV/c)^2 .

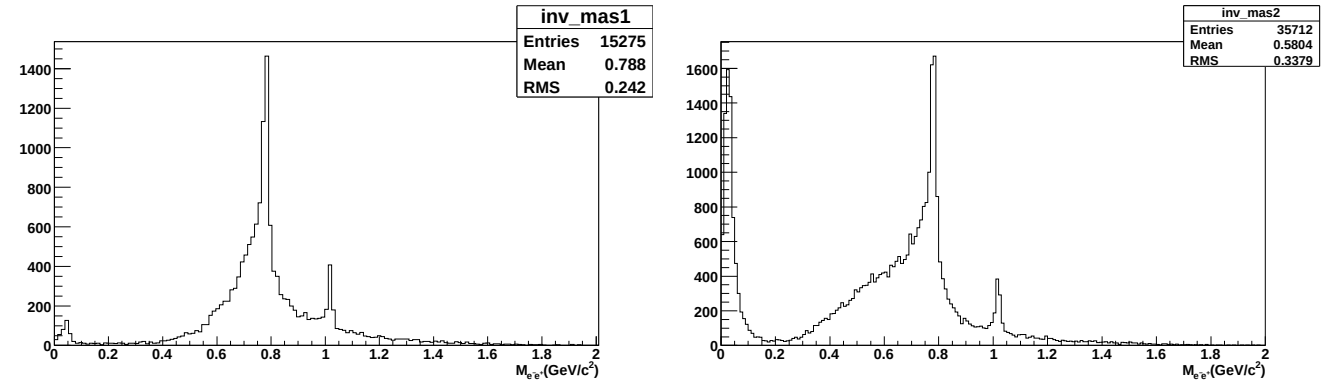

FIG. 13: Invariant mass distribution of (e^+e^-) pairs for e1-6 (left) and e1f (right).

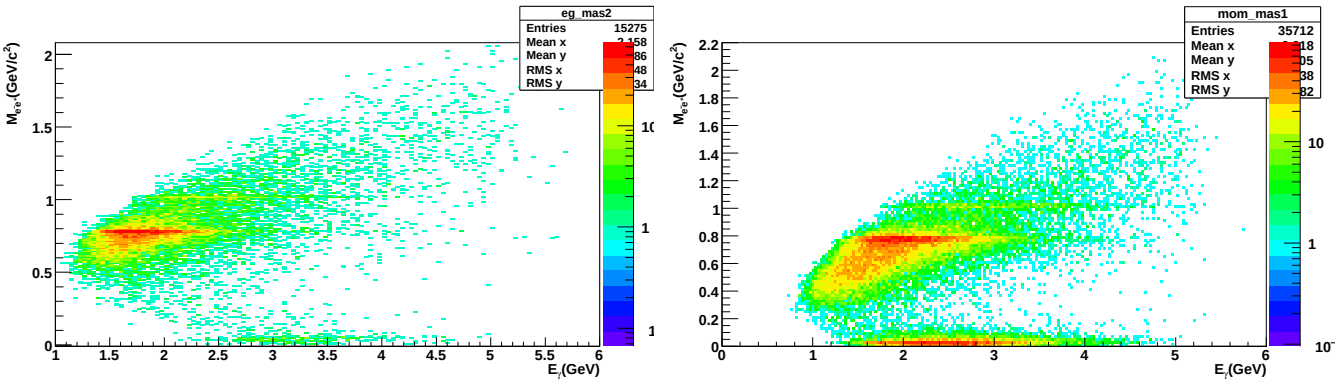

FIG. 14: Distribution of (e^+e^-) invariant mass as a function of quasi-real photon energy for e1-6, (left) and e1f (right).

VI. TCS ANALYSIS

As was mentioned above, events with $M_{e^+e^-} = Q' > 1.2$ GeV in the reaction $\gamma p \rightarrow e^+e^-p$ were selected for TCS analysis. The goal of the analysis is to extract experimental ratios of weighted cross sections, R, as presented in Eq.(18). The available statistics can be seen in the t-distributions of events shown in Fig. 15. In order to construct the ratio R, weighted yields will be calculated by integrating events in the range of c.m. polar angle θ of e^- after acceptance corrections:

$$\frac{dY}{dQ'^2\, dt\, d\varphi} = \sum_{\theta} \frac{L(\theta,\varphi)}{L_0(\theta)} \frac{N}{\Delta Q'^2\, \Delta t\, \Delta\varphi} \frac{1}{\varepsilon}\,, \tag{21}$$

where ε is the detector efficiency for detecting (e^+e^-p) in the kinematical bin of $\Delta Q'^2$, Δt, $\Delta\varphi$, and $\Delta\theta$, and $L(\theta,\varphi)$ and $L_0(\theta)$ are obtained using Eq. (15) and Eq. (16).

The coverage in θ for events in the t-range $|t| < 0.5$ is shown in Fig.16. The weighted yields of events (without acceptance corrections) are shown in Fig.17.

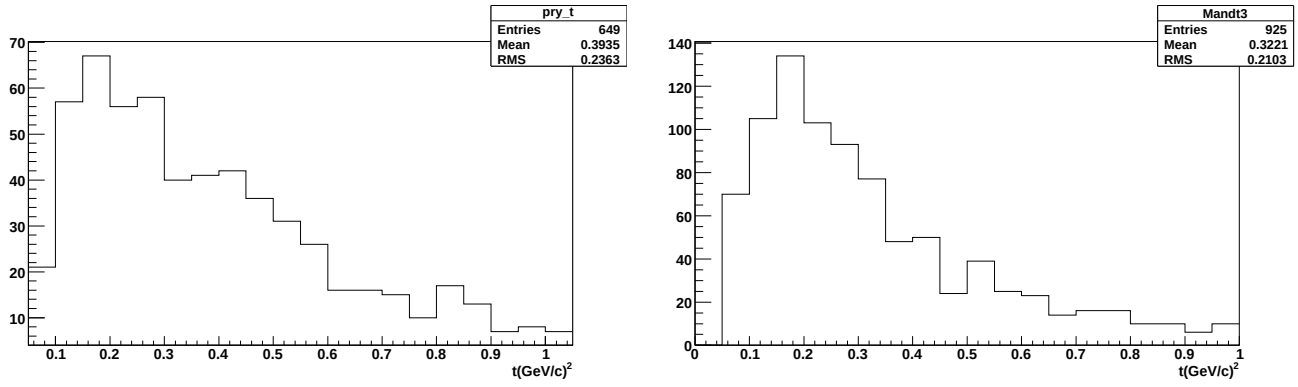

FIG. 15: t-distributions of TCS events with $Q' > 1.2$ GeV/c^2 from e1-6 (left) and e1f (right) data sets.

The experimental ratio R will be calculated as:

$$R(\sqrt{s},\ Q'^2,\ t) = \frac{\sum_{\varphi} cos\varphi \frac{dY}{dQ'^2\, dt\, d\varphi}}{\sum_{\varphi} \frac{dY}{dQ'^2\, dt\, d\varphi}}\,. \tag{22}$$

VII. SUMMARY AND OUTLOOK

In this analysis, Timelike Compton Scattering is studied using the CLAS e1-6 and e1f data sets. Quasi-real photoproduction of heavy lepton pairs is identified by requiring the undetected scattered

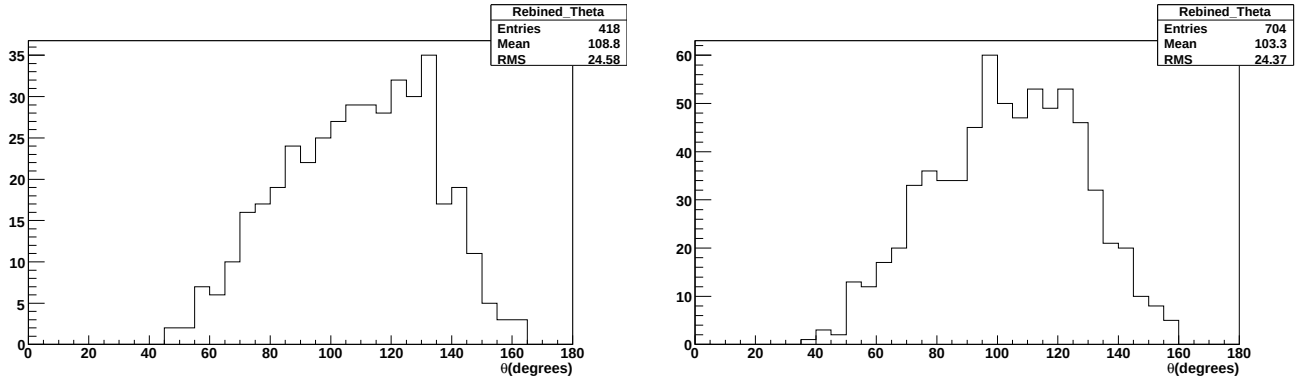

FIG. 16: Distributions of TCS events in θ angle for e1-6, (left) and e1f (right) data sets.

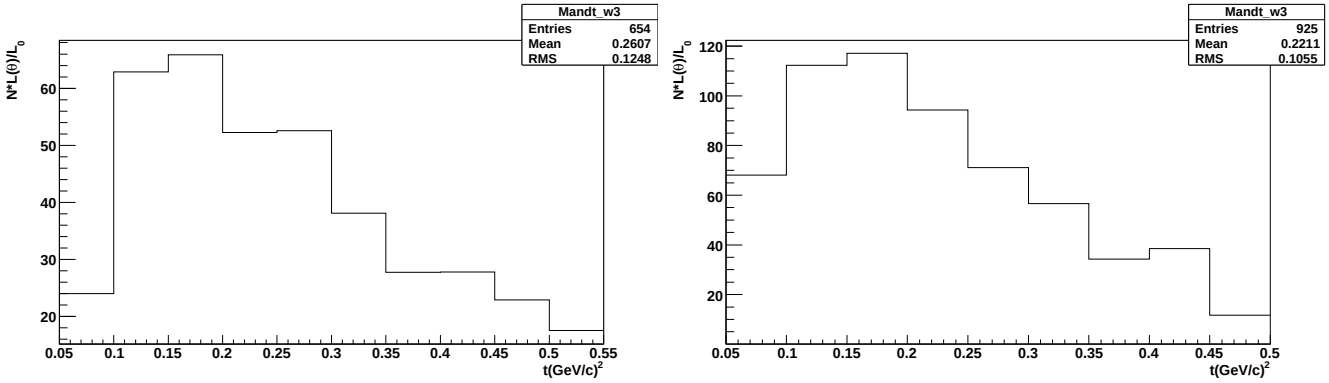

FIG. 17: t-distributions weighted by $L(\theta)/L_0$ for TCS events in e1-6, (left) and e1f (right) data sets.

electron to be at approximately zero degrees. The $\cos\phi$ moment of the BH-TCS interference part, which depends on linear combinations of real part of GPDs $\mathcal{H}$, $\tilde{\mathcal{H}}$, and $\mathcal{E}$, will be extracted using the ratio of the weighted yields.

The analysis is at a quite advanced stage. Full statistics from both data sets is being already analyzed, and $ep \rightarrow e^+e^-p'(e')$ events have been skimmed. Some more work on PID is needed. For cleaning the electron/positron sample, cuts on the absolute energy in the inner part of the EC will be studied. For protons, vertex time distributions will be analyzed. Reduction and estimates of systematic uncertainties will be done. Study of background contributions due to other physics

channels will be performed.

The next step will be to develop fiducial cuts and momentum corrections, and perform acceptance calculations. Since there is no need for absolute cross section calculations, only ratios will be studied, fiducial acceptances will be used to extract weighted yields.

---

[1] X. Ji, Phys. Rev. Lett. **78**, 610 (1997); Phys. Rev. D **55**, 7114 (1997).

[2] A.V. Radyushkin, Phys. Lett. **B380**, 417 (1996); Phys. Rev. D **56**, 5524 (1997).

[3] M. Burkardt, Phys. Rev. **D62**, 071503 (2000).

[4] J. Gronberg et al. (CLEO Collaboration), Phys. Rev. **D57**, 33 (1998).

[5] A.P. Bakulev, K. Passek-Kumericki, W. Schroers, and N.G. Stefanis, Phys. Rev. **D70**, 033014 (2004).

[6] A. Belitsky, X.-d. Ji, and F. Yuan, Phys. Rev. Lett. **91**, 092003 (2003).

[7] J.C. Collins, L. Franfurt, and M. Strikman, Phys. Rev. D **56**, 2982 (1997).

[8] A. Radyushkin, Phys. Rev. D**59**, 014030 (1999).

[9] M. Polyakov, and C. Weiss, Phys. Rev. **D60**, 114017 (1999).

[10] M. Guidal, M. Polyakov, A. Radushkin, and M. Vanderhaeghen, Phys. Rev. **D72**, 054013 (2005).

[11] M. Diehl T. Gousset, B. Pire and J.P. Ralston, Phys. Lett. **B411**, p193 (1997).

[12] A.V. Belitsky, D. Müller, and A. Kirchner, Nucl.Phys. **B629**, p323 (2002).

[13] S. Stepanyan et al., Phys. Rev. Lett. **87**, 182002 (2001).

[14] A. Airapetian et al., Phys. Rev. Lett. **87**, 182001 (2001).

[15] S. Chen et al., Phys. Rev. Lett. **97**, 072002 (2006).

[16] C. Munoz Camacho et al., Phys. Rev. Lett. **97**, 262002, (2006).

[17] M. Mazouz et al., Phys.Rev.Lett. **99**, 242501 (2007).

[18] A. Airapetian et al., (HERMES Collaboration), Phys.Rev. **D 75**, 011103 (2007).

[19] F.X. Girod et al., Phys. Rev. Lett. **100**, 162002 (2008)

[20] C. Adloff et al., Phys.Lett. **B 517**, 47 (2001);
S. Chekanov et al., Phys.Lett. **573**, 46 (2003);
A. Aktas et al., Eur.Phys.J. **C 44**, 1 (2005).

[21] F. Ellinghaus et al., Eur.Phys.J. **C 46**, 729 (2006);
Z. Ye, (HERMES Collaboration), ArXiv:hep-ex/0606061.

[22] M. Guidal, Eur.Phys.J. **A37**, p319 (2008).

[23] M. Guidal and M. Vandehaghen, Phys.Rev.Lett. **90**, 012001 (2003).

[24] A.V. Belitsky and D. Müller, Phys.Rev.Lett. **90**, 022001 (2003).

[25] E.R. Berger, M. Diehl and B. Pire, Eur.Phys.J. **C 23**, p675 (2002).

[26] B. Pire, L. Szymanowski and J. Wagner, Phys. Rev. D **79**, 014010 (2009)

[27] S. Morrow, M. Guidal, and M. Garçon, Presentations at the CLAS physics working group meetings.

[28] Particle Data Group, Physics Letter **B667** (2008).

[29] M. Wood et al.(The CLAS Collaboration), Phys.Rev. **C78** 015201, (2008).